Diffusion of Ferrocene through Vanadyl Phosphate by Density Functional
Theory (Supporting Information)

Yuan Liu (刘源)[1], An T. Ta[1], R. Seaton Ullberg[1], Jiahui Liu[2], Daniel R. Talham[2]
and Simon R. Phillpot[1*]
[1]Department of Materials Science and Engineering, University of Florida,
Gainesville FL 32611 USA
[2]Department of Chemistry, University of Florida, Gainesville FL 32611 USA

To be submitted to Physical Chemistry Chemical Physics

Table of Contents

Effect of Spring Constant on NEB Barriers

We tested four different spring constants, -0.5 eV/Å^2, -3 eV/Å^2, -5 eV/Å^2 and -7 eV/Å^2.
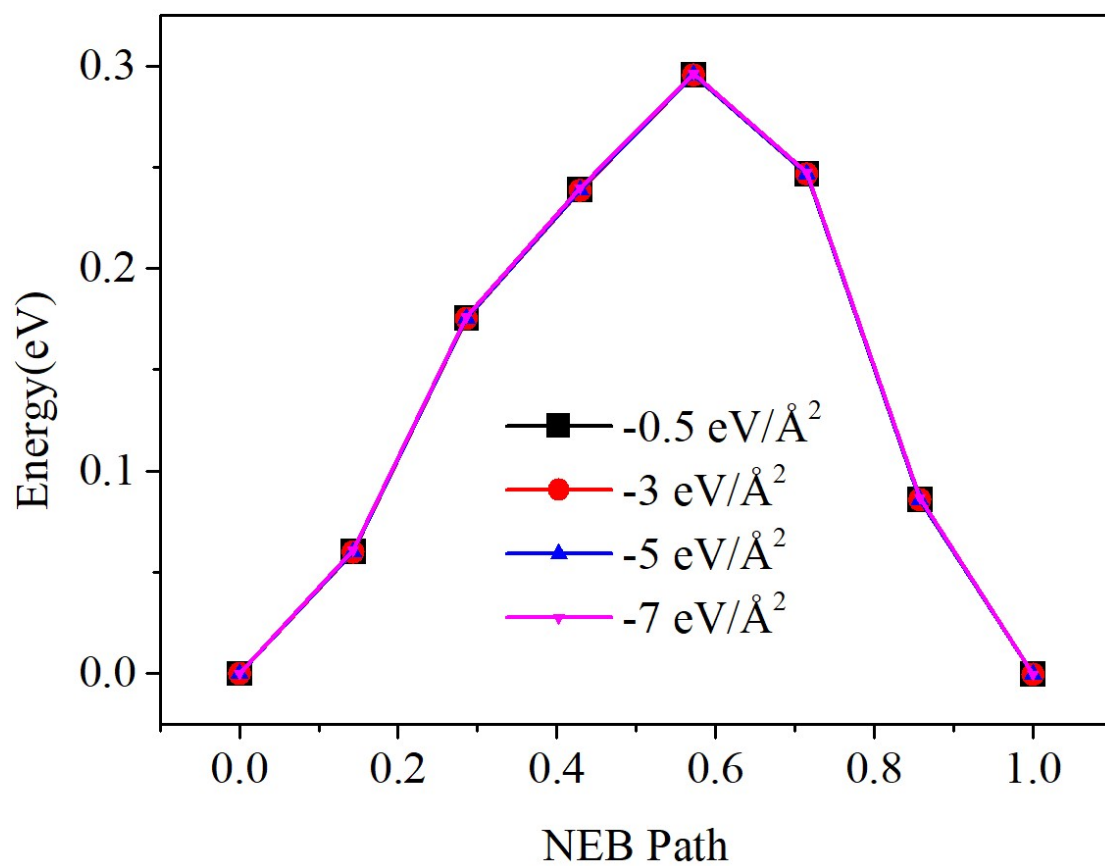The NEB energy barriers are independent of the spring constant. See Figure S1 below.

Figure S1. Evaluation of the effect of spring constant on NEB calculations for E-V-45°
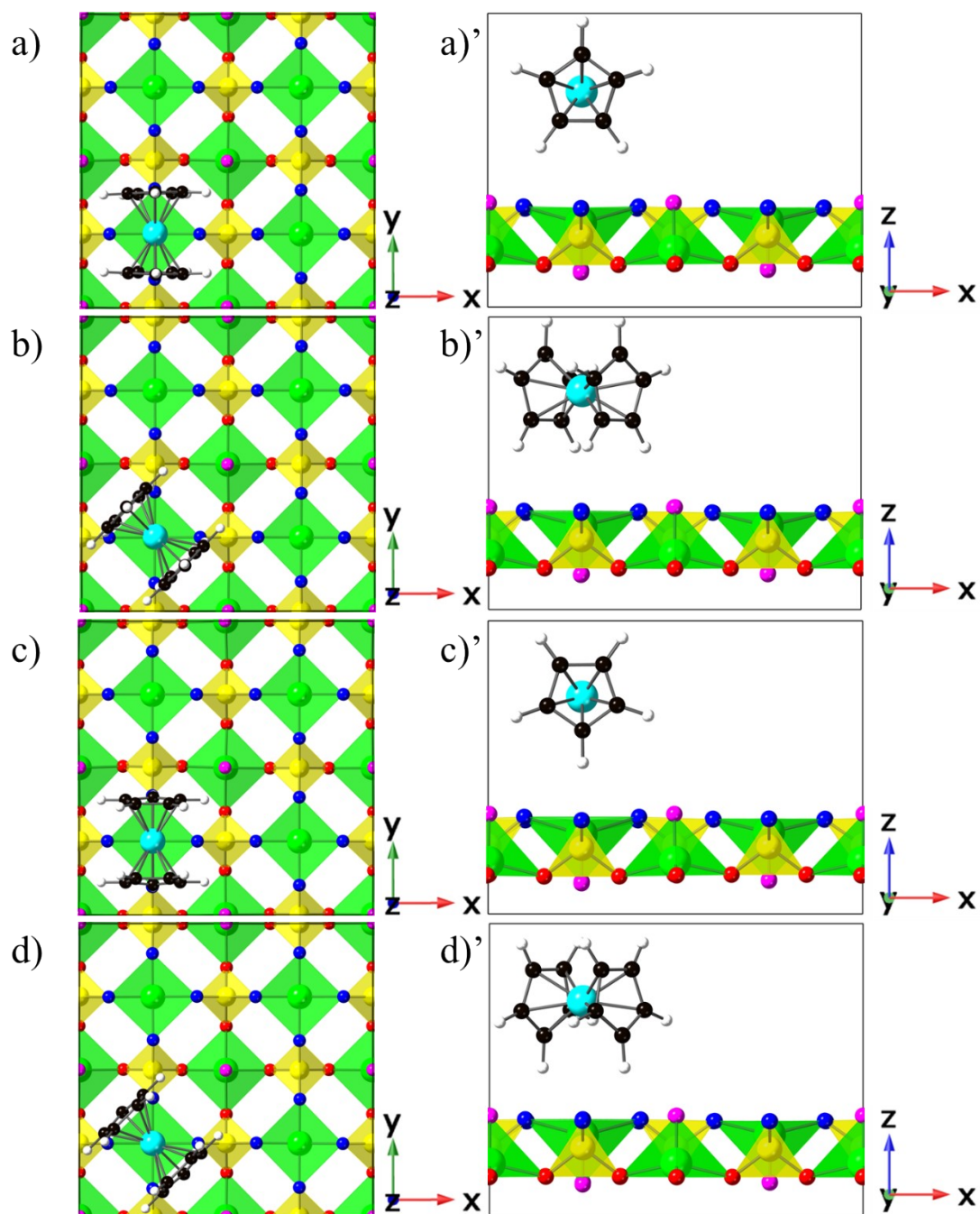to E-V-45° path.

Intercalation Configurations

Figure S2. The configurations of a) E-VO-0°, b) E-VO-45°, c) E-V-0° and d) E-V-45° are viewed along the [001] direction. The corresponding pictures denoted with prime (') are viewed along the [010] direction. All subsequent configurations are shown in the same directions as these ones. The black box is the unit cell.

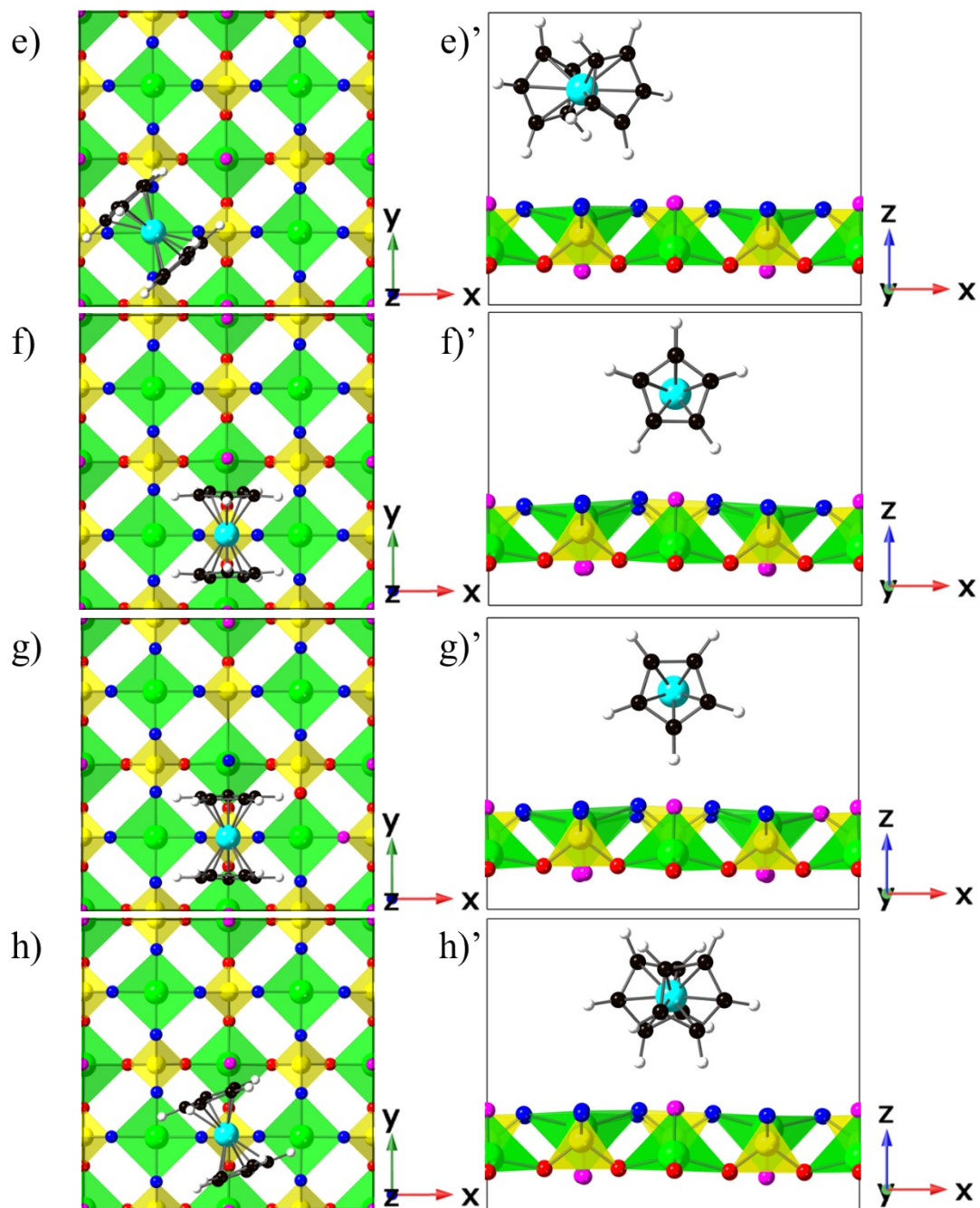**Figure S2.** The configurations of e) S-V-45°, f) E-P$_{VO}$-0°, g) E-P$_V$-0° and h) G-P-20° are viewed along the [001] direction. The corresponding pictures denoted with prime (') are viewed along the [010] direction. The black box is the unit cell.

Density of States

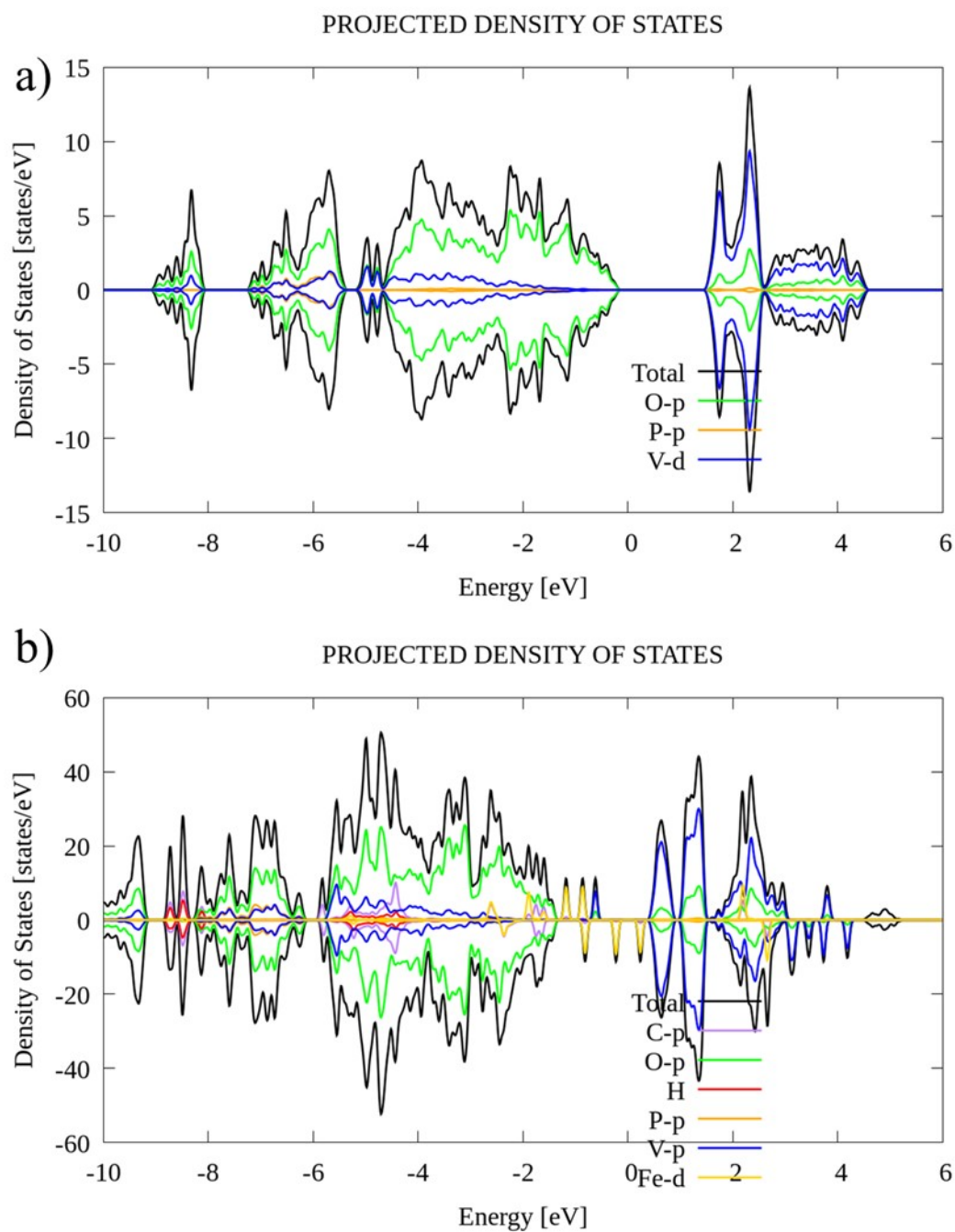## PROJECTED DENSITY OF STATES

a)

b)

Figure S3. a) Pristine VOPO4 DOS, and b) Intercalated Ferrocene-VOPO$_4$ DOS.

The density of states (DOS) for both the pristine VOPO$_4$ and the intercalated ferrocene-VOPO$_4$ phases (E-V-45°). The DOS plots are shown in Figures S3.

1. **Band Gap Reduction:**

o Pristine $VOPO_4$: The pristine $VOPO_4$ exhibits a clear band gap of approximately 2 eV, characteristic of a semiconductor.

o Intercalated Ferrocene-$VOPO_4$: Upon intercalation with ferrocene, the band gap significantly reduces to about 0.5 eV. This substantial reduction in band gap indicates that the material transitions towards a more conductive state. The narrowing of the band gap is primarily due to the introduction of new electronic states by the ferrocene molecules.

2. **Elemental Contributions:**

o Pristine $VOPO_4$: The DOS shows that the O-p orbitals (green) contribute significantly in the energy range from -8 eV to -2 eV, while the V-d orbitals (blue) dominate near the conduction band (2 eV to 4 eV). The P-p orbitals (orange) also contribute within the valence band but to a lesser extent.

o Intercalated Ferrocene-$VOPO_4$: The introduction of ferrocene leads to new states primarily from the Fe-d orbitals (yellow) near the Fermi level. This inclusion results in increased electronic states around the Fermi level, contributing to the observed decrease in the band gap. The O-p and P-p orbitals continue to show significant contributions in the valence band, while the V-d orbitals remain significant in the conduction band.

3. **Electronic Structure and Conductivity:**

o The drastic reduction in the band gap upon ferrocene intercalation suggests a transition from semiconducting to a more metallic or highly conductive behavior. This is supported by the increased density of states at the Fermi level, indicating that electrons can more easily be excited to the conduction band, enhancing the material's conductivity.

o The presence of Fe-d states at the Fermi level introduces additional pathways for electron conduction, which could be beneficial for applications requiring high electrical conductivity.

The calculated DOS for pristine and intercalated $VOPO_4$ phases reveals significant changes in electronic structure upon ferrocene intercalation. The band gap reduction and the increased density of states at the Fermi level imply enhanced electronic conductivity, which could be advantageous for various electronic and electrochemical applications.
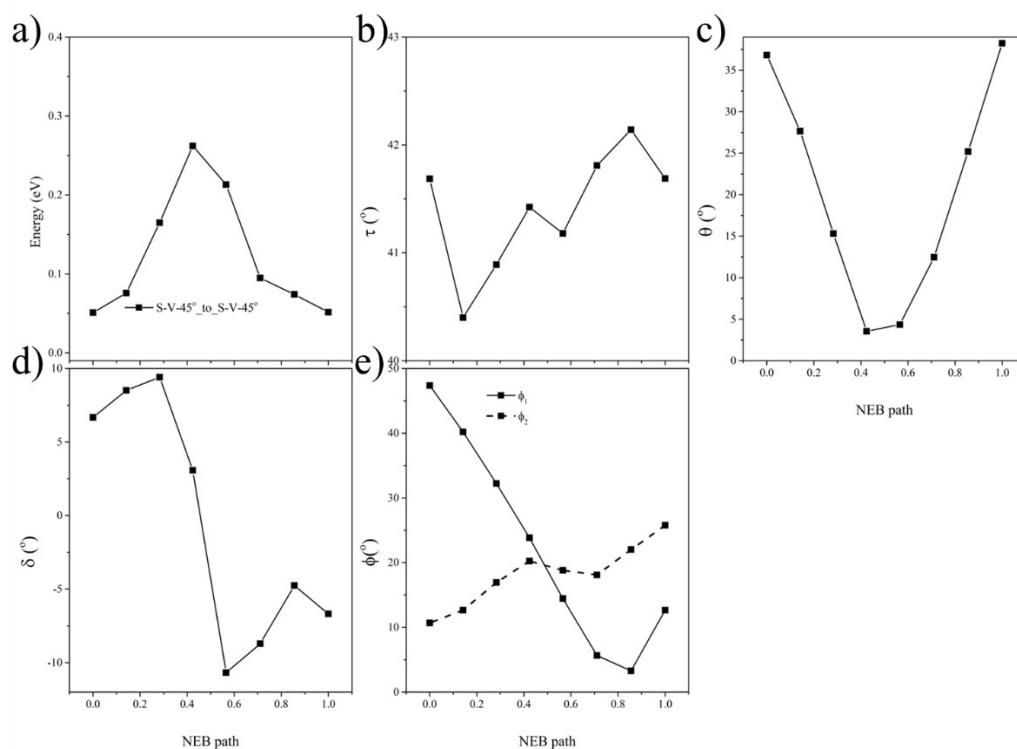
Sliding Only: V→V[110].

Figure S4. a) NEB energy profiles for pathways S-V-45º to S-V-45º; b) rotational angle variations of ferrocene; c) changes in the angle between -CH bonds in the cyclopentadienyl rings; d) dihedral angle adjustments between the cyclopentadienyl rings; e) orientation of -CH bonds relative to the [001] direction for the S-V-45º to S-V-45º path.

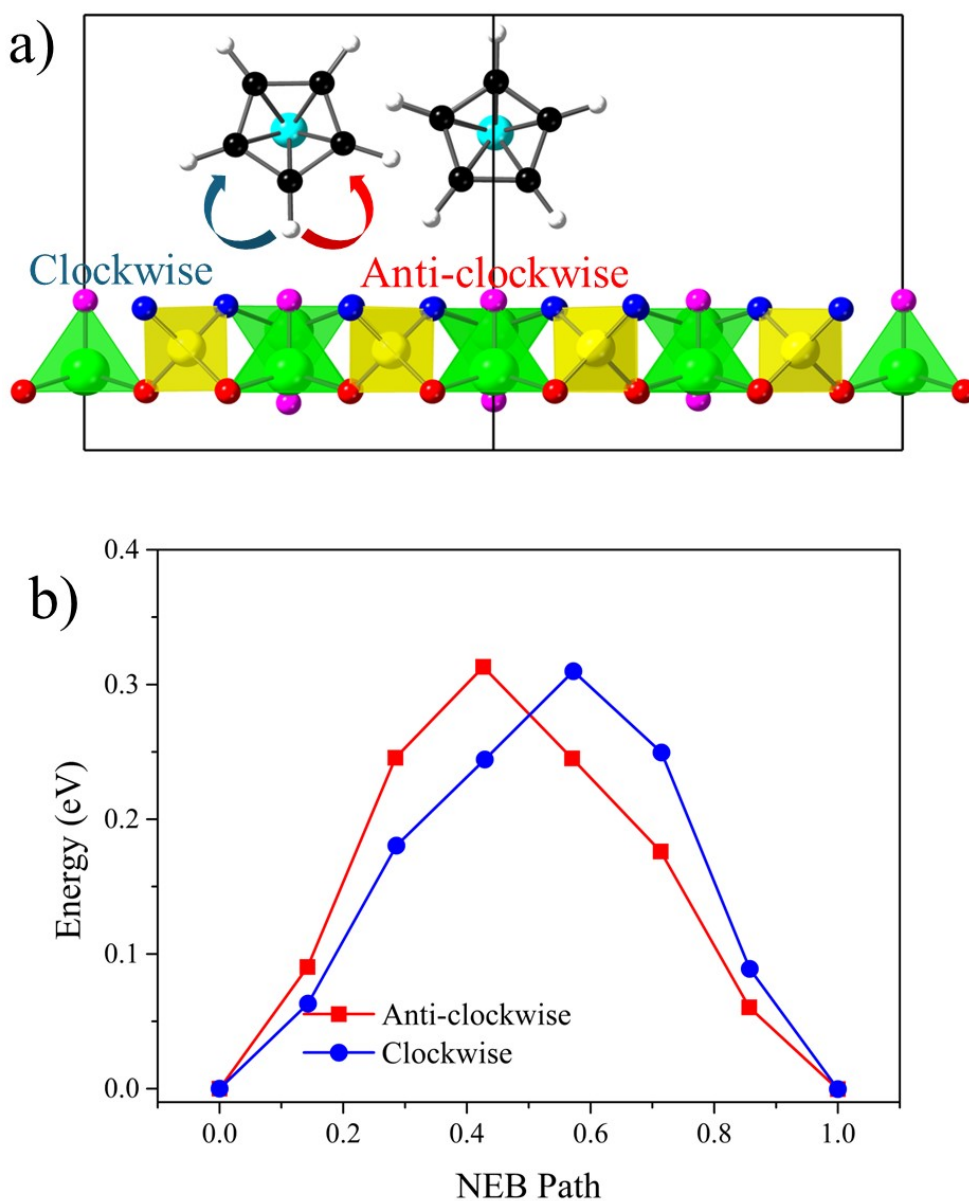# Rolling Direction Effect: Clockwise vs. Anti-clockwise)

Figure S5. a) The E-V-45º to E-V-45º path along the [110] direction. The blue curved arrow means the ferrocene is rolling clockwise during diffusion, while red curved arrow means anti-clockwise; b) The NEB energy profile of ferrocene rolling on E-V-45º to E-V-45º.
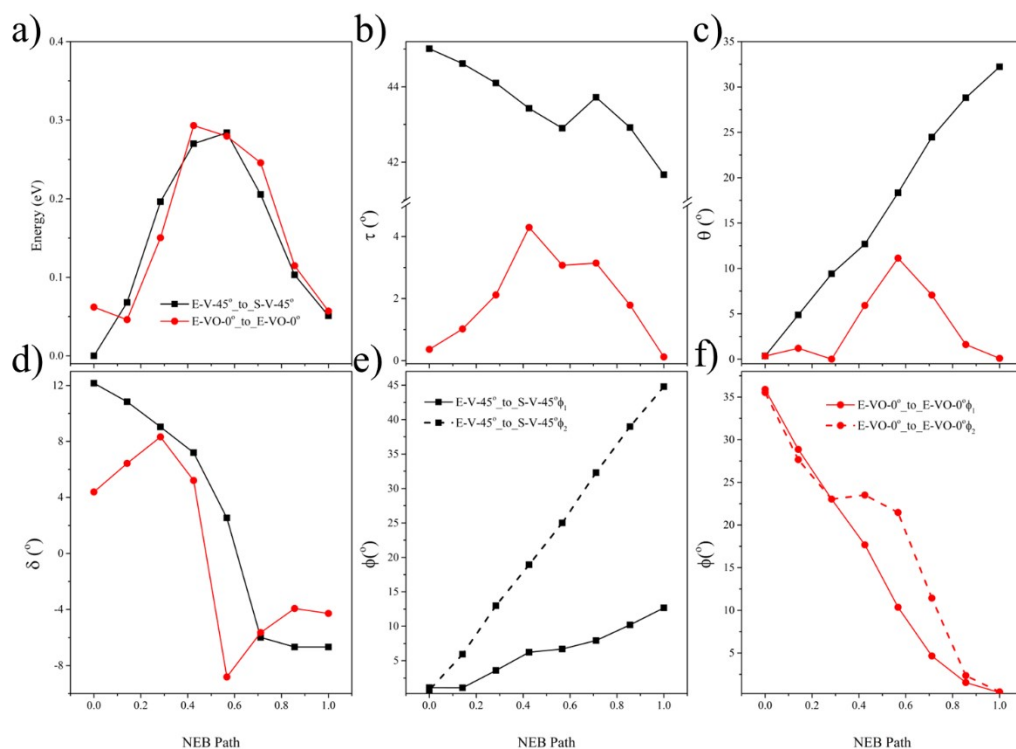
Sliding + Rolling: V➔V[110].

Figure S6. (a) NEB energy profiles for pathways E-V-45º to S-V-45º (black) and E-VO-0º to E-VO-0º (red); (b) rotational angle variations of ferrocene; (c) changes in the angle between -CH bonds in the cyclopentadienyl rings; (d) dihedral angle adjustments between the cyclopentadienyl rings; (e) orientation of -CH bonds relative to the [001] direction for the E-V-45º to S-V-45º path; and (f) orientation of -CH bonds relative to the [001] direction for the E-VO-0º to E-VO-0º path.
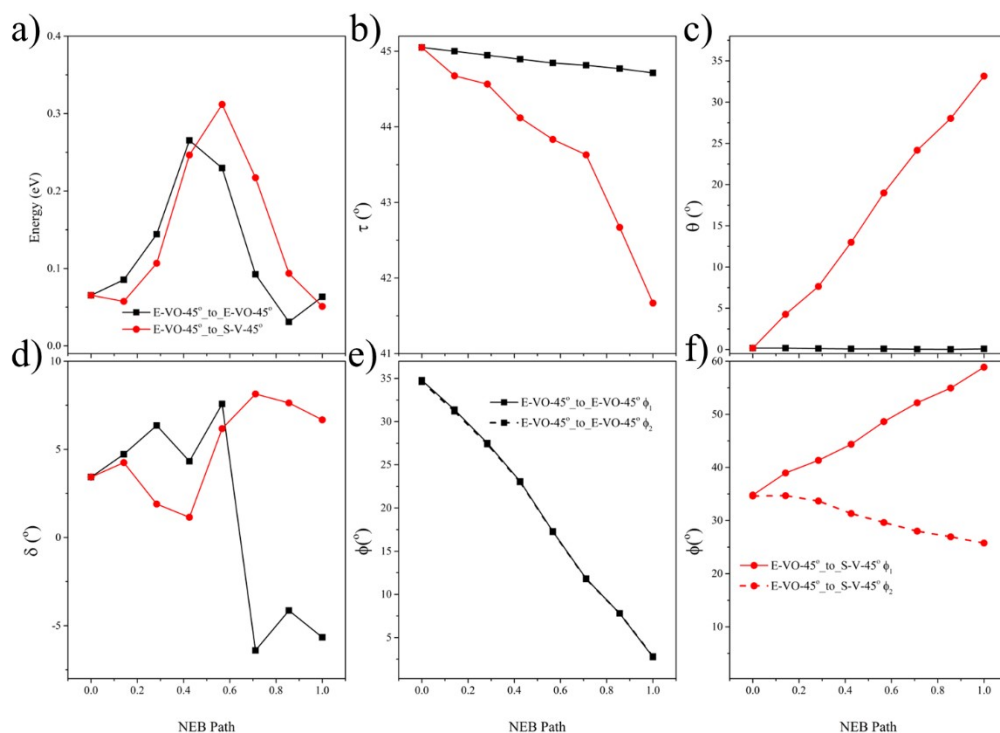
Figure S7. (a) NEB energy profiles for pathways E-VO-45º to E-VO-45º (black) and E-VO-45º to S-V-45º (red); (b) rotational angle variations of ferrocene; (c) changes in the angle between -CH bonds in the cyclopentadienyl rings; (d) dihedral angle adjustments between the cyclopentadienyl rings; (e) orientation of -CH bonds relative to the [001] direction for the E-VO-45º to E-VO-45º path; and (f) orientation of -CH bonds relative to the [001] direction for the E-VO-45º to S-V-45º path.

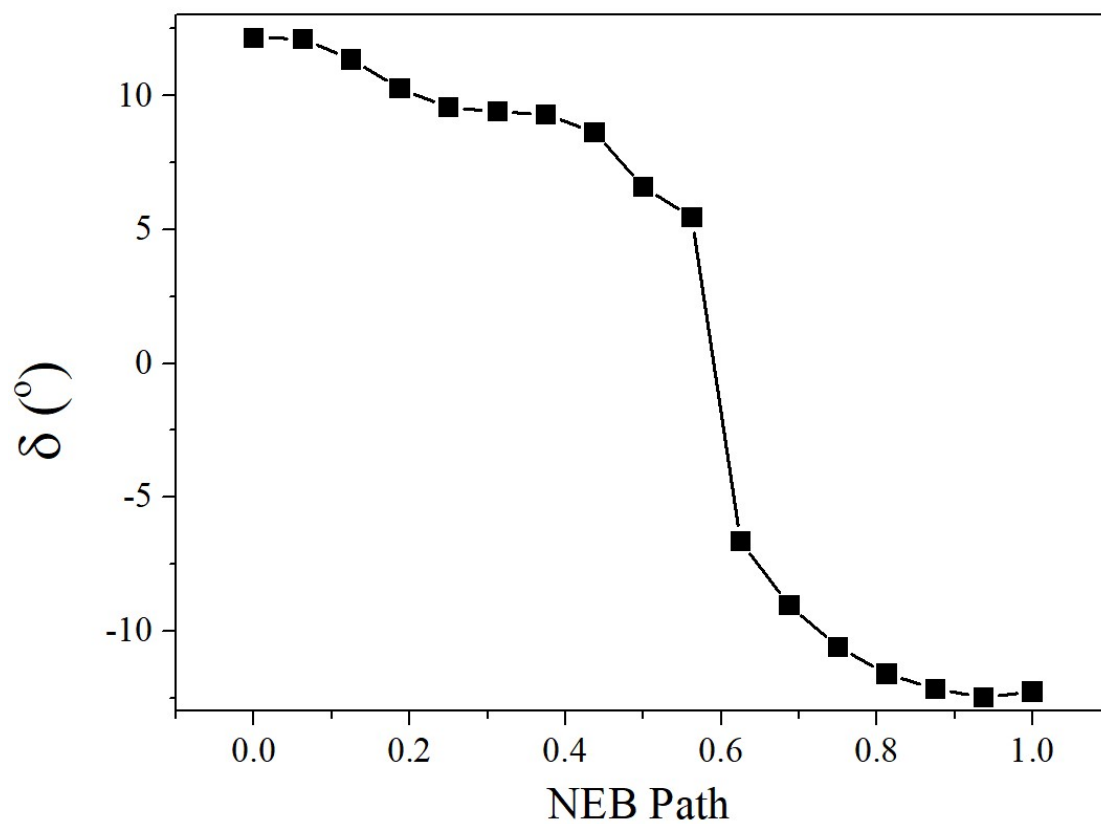# Denser Images of Dihedral Angle for E-V-45º to E-V-45º.

Figure S8. Dihedral angle measurements between the cyclopentadienyl rings of E-V-45º to E-V-45º path with more images.
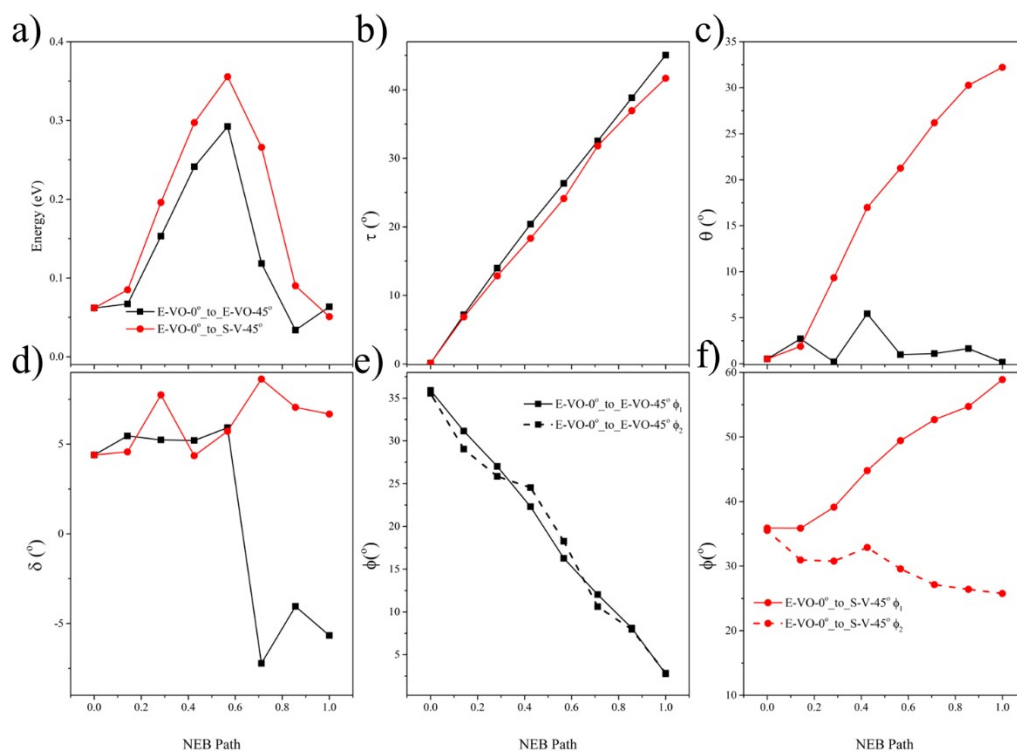
Sliding + Rotation + Rolling: V→V[110].

Figure S9. (a) NEB energy profiles for pathways E-VO-0º to E-VO-45º (black) and E-VO-0º to S-V-45º (red); (b) rotational angle variations of ferrocene; (c) changes in the angle between -CH bonds in the cyclopentadienyl rings; (d) dihedral angle adjustments between the cyclopentadienyl rings; (e) orientation of -CH bonds relative to the [001] direction for the E-VO-0º to E-VO-45º path; and (f) orientation of -CH bonds relative to the [001] direction for the E-VO-0º to S-V-45º path.
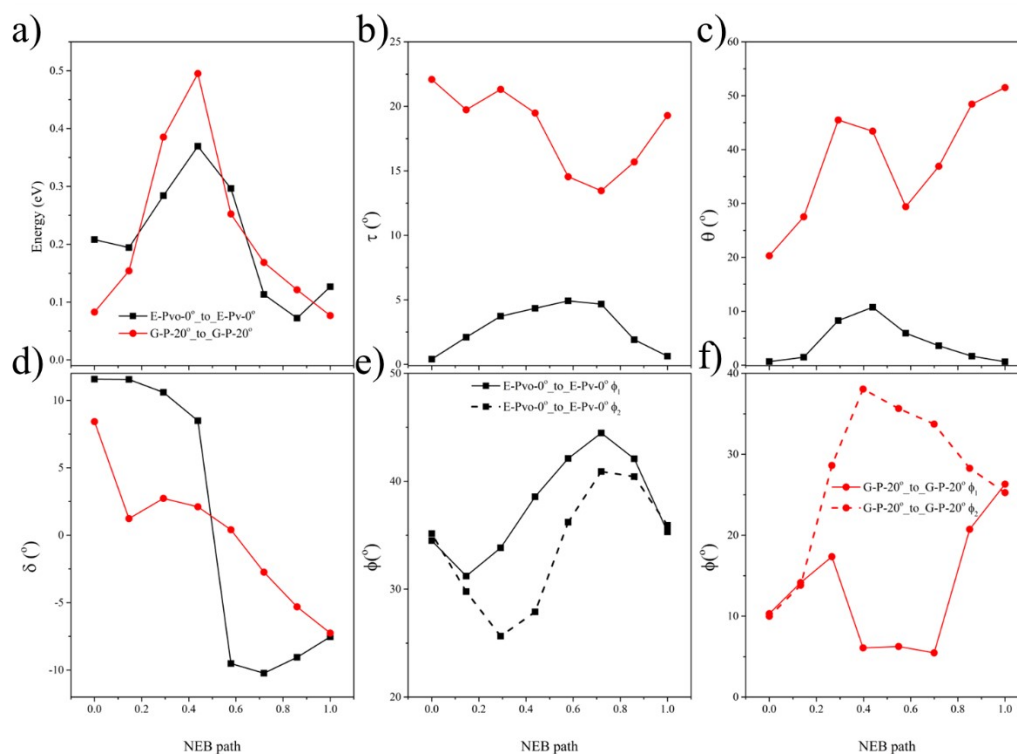
Sliding Only: P→P [110]

Figure S10. (a) NEB energy profiles for pathways E-Pvo-0º to E-Pv-0º (black) and G-P-20º to G-P-20º (red); (b) rotational angle variations of ferrocene; (c) changes in the angle between -CH bonds in the cyclopentadienyl rings; (d) dihedral angle adjustments between the cyclopentadienyl rings; (e) orientation of -CH bonds relative to the [001] direction for the E-Pvo-0º to E-Pv-0º path; and (f) orientation of -CH bonds relative to the [001] direction for the G-P-20º to G-P-20º path.
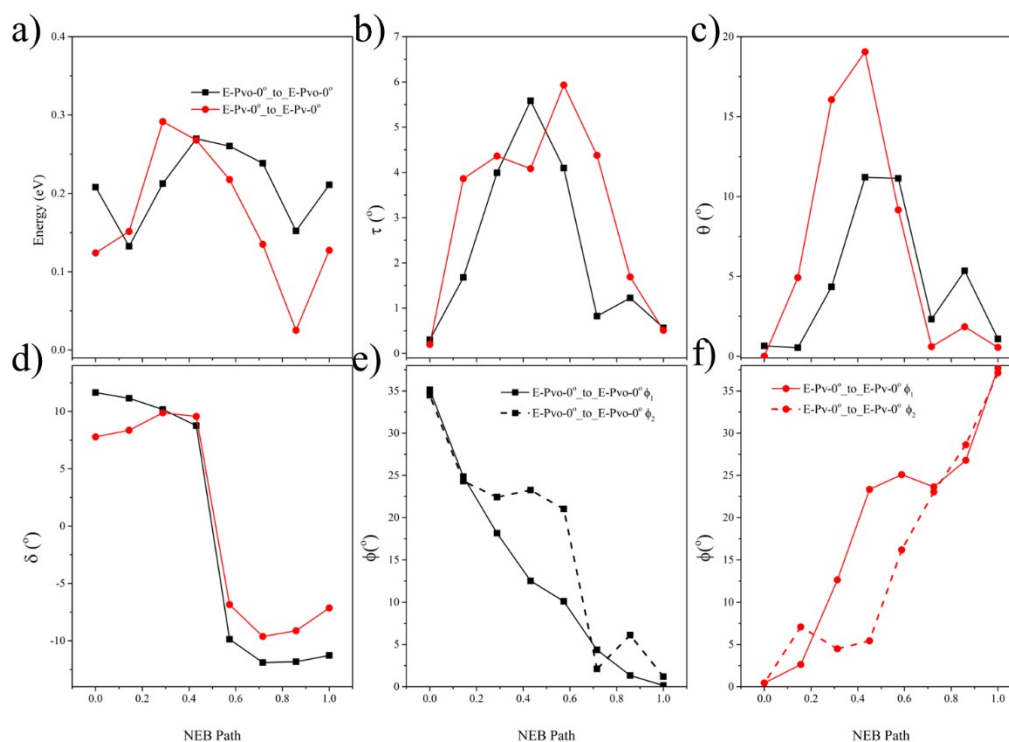
Sliding + Rolling: P➔P[110].

Figure S11. (a) NEB energy profiles for pathways E-Pvo-0º to E-Pvo-0º (black) and E-Pv-0º to E-Pv-0º (red); (b) rotational angle variations of ferrocene; (c) changes in the angle between -CH bonds in the cyclopentadienyl rings; (d) dihedral angle adjustments between the cyclopentadienyl rings; (e) orientation of -CH bonds relative to the [001] direction for the E-Pvo-0º to E-Pvo-0º path; and (f) orientation of -CH bonds relative to the [001] direction for the E-Pv-0º to E-Pv-0º path.
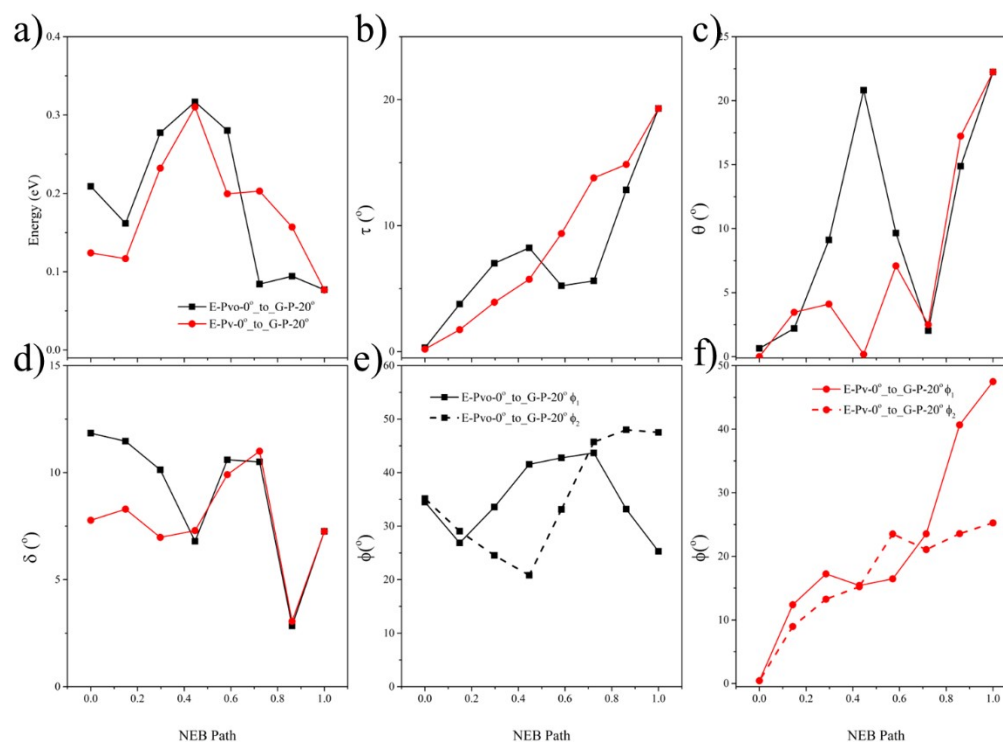
Sliding + Rotation + Rolling: P→P[110].

Figure S12. (a) NEB energy profiles for pathways E-Pvo-0º to G-P-20º (black) and E-Pv-0º to G-P-20º (red); (b) rotational angle variations of ferrocene; (c) changes in the angle between -CH bonds in the cyclopentadienyl rings; (d) dihedral angle adjustments between the cyclopentadienyl rings; (e) orientation of -CH bonds relative to the [001] direction for the E-Pvo-0º to G-P-20º path; and (f) orientation of -CH bonds relative to the [001] direction for the E-Pv-0º to G-P-20º path.
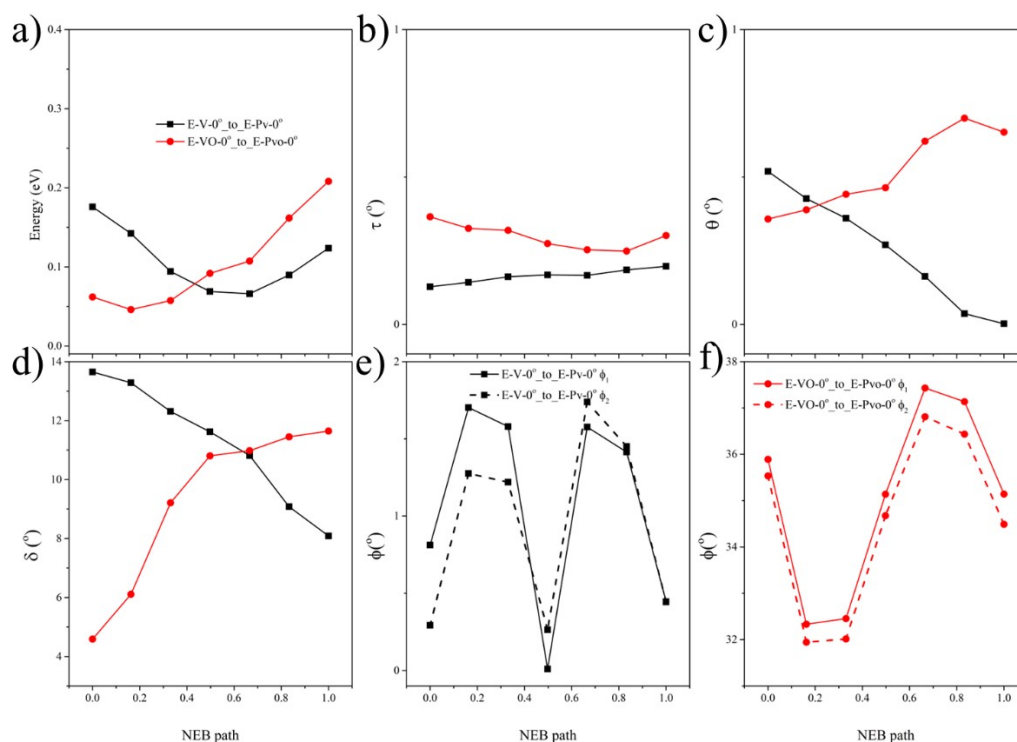
Sliding Only: V➔P[100].

Figure S13. (a) NEB energy profiles for pathways E-V-0º to E-Pv-0º (black) and E-VO-0º to E-Pvo-0º (red); (b) rotational angle variations of ferrocene; (c) changes in the angle between -CH bonds in the cyclopentadienyl rings; (d) dihedral angle adjustments between the cyclopentadienyl rings; (e) orientation of -CH bonds relative to the [001] direction for the E-V-0º to E-Pv-0º path; and (f) orientation of -CH bonds relative to the [001] direction for the E-VO-0º to E-Pvo-0º path.
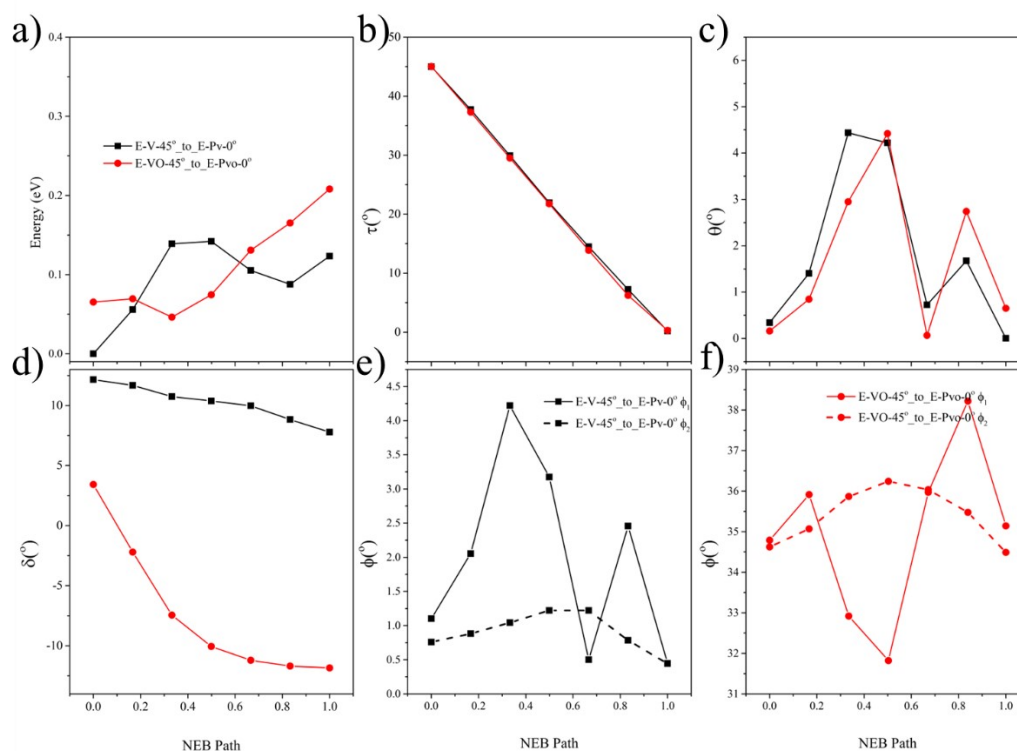
Sliding + Rotation: V→P[100].

Figure S14. (a) NEB energy profiles for pathways E-V-45º to E-Pv-0º (black) and E-VO-45º to E-Pvo-0º (red); (b) rotational angle variations of ferrocene; (c) changes in the angle between -CH bonds in the cyclopentadienyl rings; (d) dihedral angle adjustments between the cyclopentadienyl rings; (e) orientation of -CH bonds relative to the [001] direction for the E-V-45º to E-Pv-0º path; and (f) orientation of -CH bonds relative to the [001] direction for the E-VO-45º to E-Pvo-0º path.
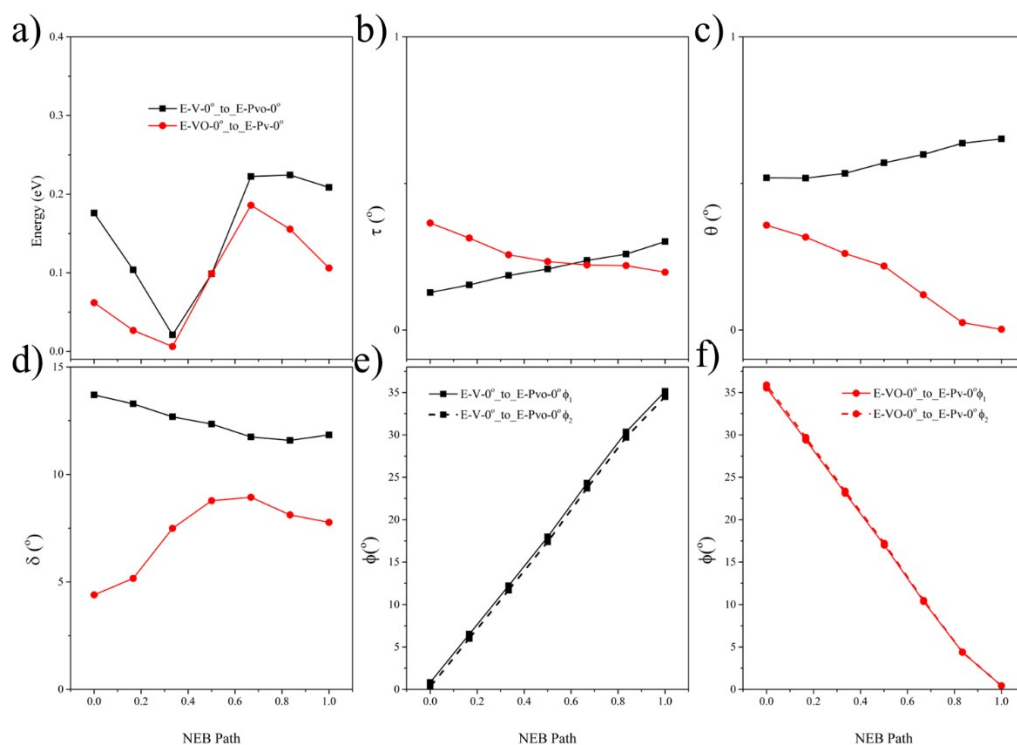
Sliding + Rolling: V➔P[100].

Figure S15. (a) NEB energy profiles for pathways E-V-0º to E-Pvo-0º (black) and E-VO-0º to E-Pv-0º (red); (b) rotational angle variations of ferrocene; (c) changes in the angle between -CH bonds in the cyclopentadienyl rings; (d) dihedral angle adjustments between the cyclopentadienyl rings; (e) orientation of -CH bonds relative to the [001] direction for the E-V-0º to E-Pvo-0º path; and (f) orientation of -CH bonds relative to the [001] direction for the E-VO-0º to E-Pv-0º path.
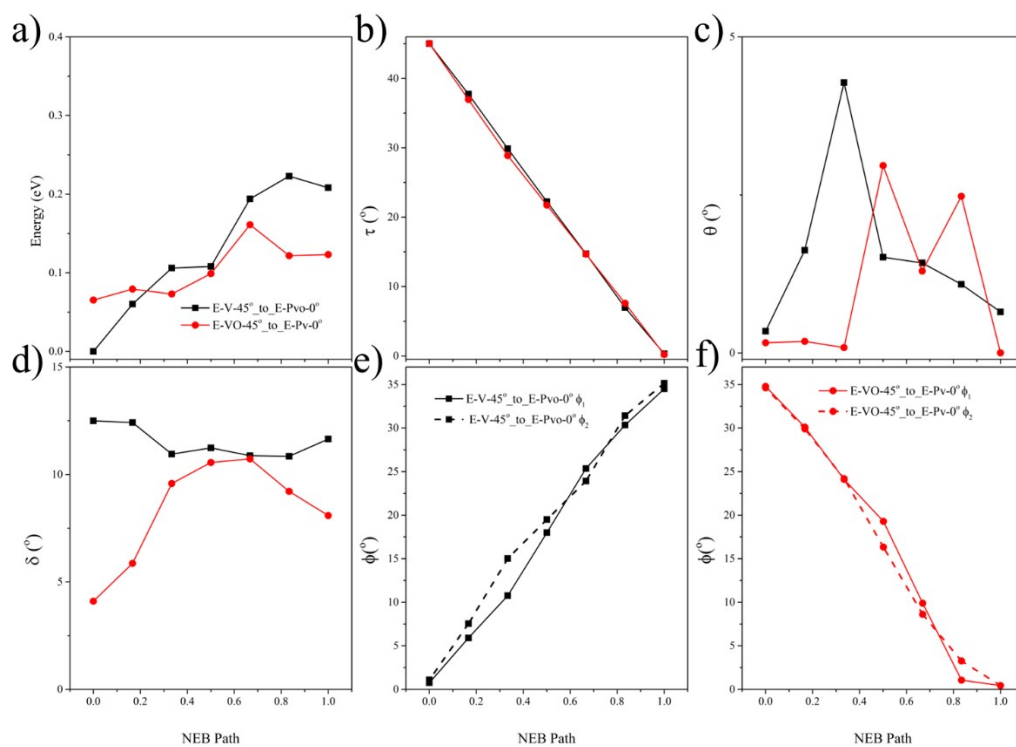
Sliding + Rolling + Rotation: V→P[110].

Figure S16. (a) NEB energy profiles for pathways E-V-45º to E-Pvo-0º (black) and E-VO-45º to E-Pv-0º (red); (b) rotational angle variations of ferrocene; (c) changes in the angle between -CH bonds in the cyclopentadienyl rings; (d) dihedral angle adjustments between the cyclopentadienyl rings; (e) orientation of -CH bonds relative to the [001] direction for the E-V-45º to E-Pvo-0º path; and (f) orientation of -CH bonds relative to the [001] direction for the E-VO-45º to E-Pv-0º path.
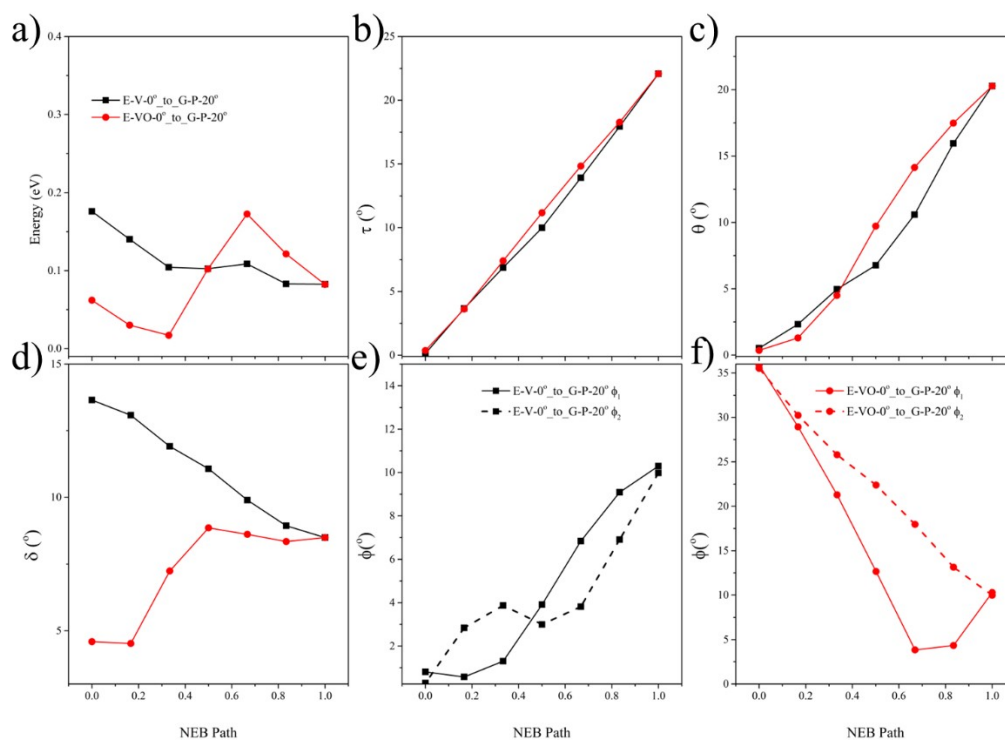
Figure S17. (a) NEB energy profiles for pathways E-V-0º to G-P-20º (black) and E-VO-0º to G-P-20º (red); (b) rotational angle variations of ferrocene; (c) changes in the angle between -CH bonds in the cyclopentadienyl rings; (d) dihedral angle adjustments between the cyclopentadienyl rings; (e) orientation of -CH bonds relative to the [001] direction for the E-V-0º to G-P-20º path; and (f) orientation of -CH bonds relative to the [001] direction for the E-VO-0º to G-P-20º path.
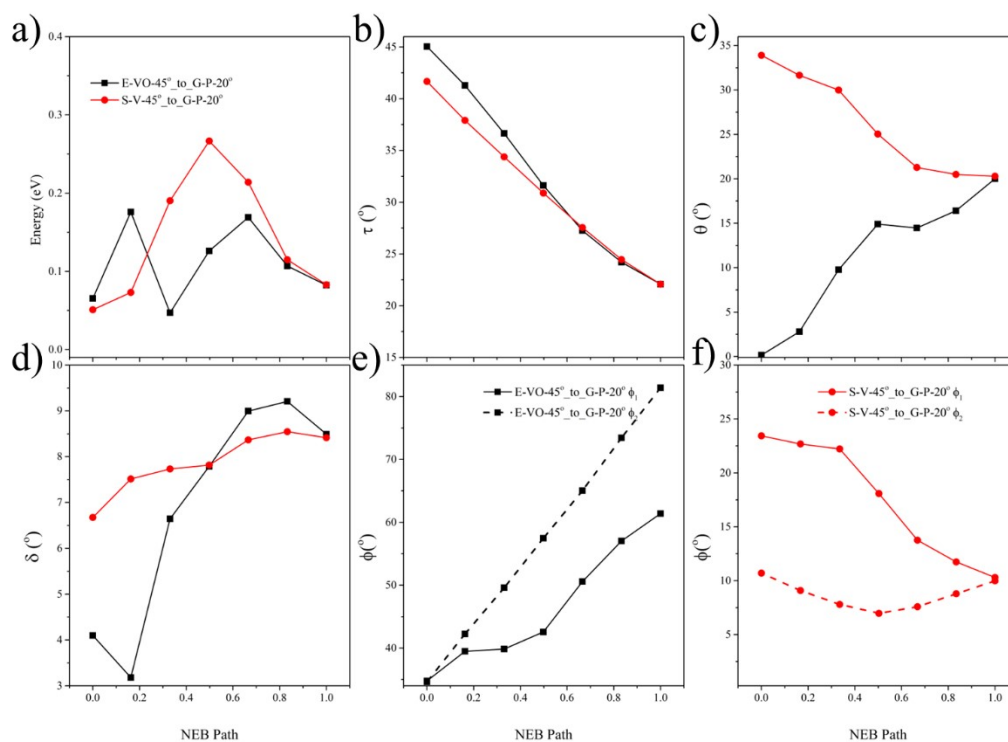
Figure S18. (a) NEB energy profiles for pathways E-VO-45º to G-P-20º (black) and S-V-45º to G-P-20º (red); (b) rotational angle variations of ferrocene; (c) changes in the angle between -CH bonds in the cyclopentadienyl rings; (d) dihedral angle adjustments between the cyclopentadienyl rings; (e) orientation of -CH bonds relative to the [001] direction for the E-VO-45º to G-P-20º path; and (f) orientation of -CH bonds relative to the [001] direction for the S-V-45º to G-P-20º path.
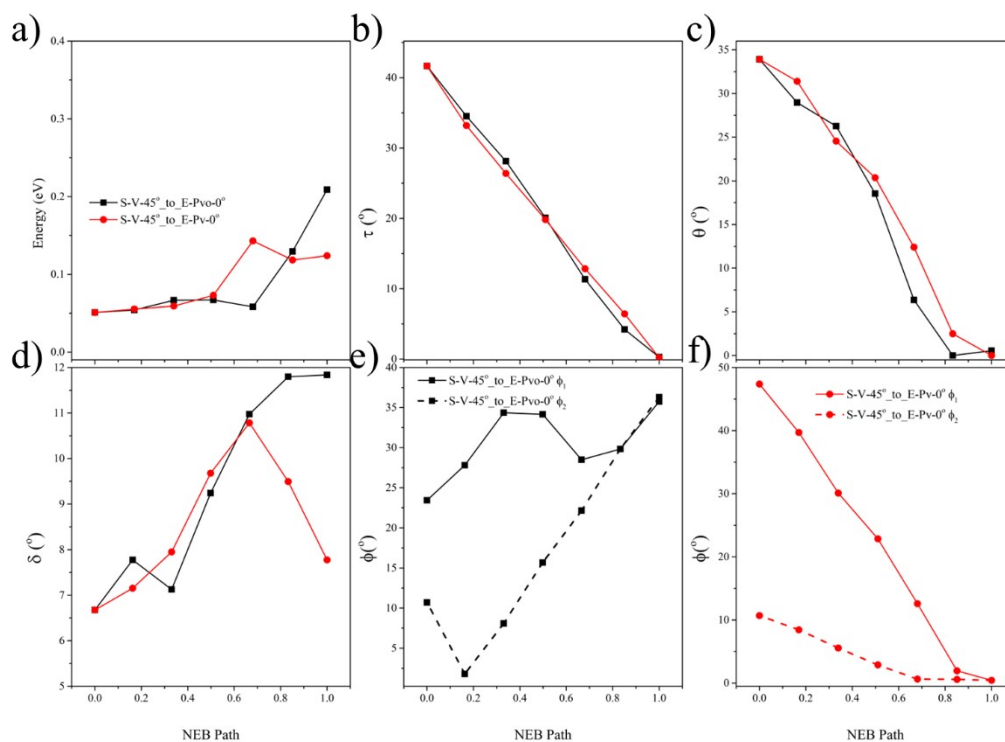
Figure S19. (a) NEB energy profiles for pathways S-V-45º to E-Pvo-0º (black) and S-V-45º to E-Pv-0º (red); (b) rotational angle variations of ferrocene; (c) changes in the angle between -CH bonds in the cyclopentadienyl rings; (d) dihedral angle adjustments between the cyclopentadienyl rings; (e) orientation of -CH bonds relative to the [001] direction for the S-V-45º to E-Pvo-0º path; and (f) orientation of -CH bonds relative to the [001] direction for the S-V-45º to E-Pv-0º path.